Whole-brain entrainment and anticipation in fMRI motor task data.

Marika Strindberg[1,*], Yu Tian[2] & Peter Fransson[1]

[1]Department of Clinical Neuroscience, Karolinska Institutet, Stockholm, Sweden.

[2] Center for Systems Biology, Dresden, Germany.

* Corresponding author
Marika Strindberg
Department of Clinical Neuroscience
Nobels väg 9
SE-171 77 Stockholm, SWEDEN
E-mail: marika.strindberg@ki.se

Themes: phase synchronization, clustering, complex network weights, attention, entrainment, fMRI.

Abstract

Evidence that the brain adapts its intrinsic rhythms to a task paradigm (entrainment) and that it actively anticipates up-coming tasks has mostly come from analysis of neurophysiological data. Here we show that these phenomena are present in fMRI motor task data as well. We represent brain activity as a series (time resolved) of complex weighted networks and introduce a novel phase clustering algorithm that divides the matrices into functionally meaningful communities with comparable phase content across time and subjects. We find brain-wide patterns of cross-subject synchronizations timed to the task paradigm. This pattern of entrainment features systematic negative deflections prior to task paradigm across many different brain regions. We interpret this pattern as a fMRI-equivalent to the Contingent Negative Variation (CNV) seen in neurophysiological data in anticipation of an up-coming task. A more pronounce version of the CNV-like signal is seen in task specific motor and somatosensory cortex prior to movement, potentially the fMRI-equivalent of the readiness potential (RP). Finally, we show that fMRI data, when represented as complex weighted matrices, full-fills the criteria of structural balance.

Introduction

A fundamental trait of the brain is its ability to predict and anticipate future events and outcomes of actions. In this predictive framework the brain is not only passively reacting to internal and external cues but preparing for the expected future and actively co-creating it (Clark 2013; Friston 2010; Buzsáki, Peyrache, and Kubie 2014; Barrett 2016; Bubic 2010). While the idea of prediction as a key feature of what the brain "does" has been around at least since Helmholtz, exactly how it is implemented is not well understood. Most of the evidence that prediction is inherent in brain processes comes from neurophysiological studies using M/EEG, where electromagnetic brain activity is typically analysed in the 1-60(0.1-100) Hz range.

Perhaps the most prominent neurophysiological marker of anticipation is a phenomenon known as the contingent negative variation (CNV). The CNV is a slow build-up of negative potential seen in M/EEG in anticipation of an up-coming task whether it be a perceptual or motor task (Brunia, Van Boxtel, and Böcker 2011). It arises in both hemispheres after an initial cue which signals that a future event is imminent. The CNV has been associated with expectation, timing, memory and decision making (Kononowicz and Penney 2016). A similar negative potential is seen in the event of an up-coming motor task even in the absence of the initial preparatory cue. It has been given a separate name, the readiness potential (RP), but it is unclear to what extent it is really a separate phenomenon (Brunia, Van Boxtel, and Böcker 2011; Schurger et al. 2021). The RP is more specific than the CNV in its spatial distribution and is observed over the supplementary motor area (SMA), premotor and primary motor cortex with a predominantly lateralized late component. The RP starts 0.5-2 s prior to self-initiated action (Schurger et al. 2021; Brunia, Van Boxtel, and Böcker 2011). In contrast, self-reports of intention to act commonly appear 200 ms before a motor action. The notion that the RP is associated with anticipation and planning has been challenged by computational models that suggest instead that is a reflection of accumulation of stochastic variability in neuronal processing (Schurger, Sitt, and Dehaene 2012). A core contributing factor to the debate of the significance and origin of the RP is the low signal to noise ratio in EEG which means that the RP is only seen after averaging across 30-40 time-locked epochs (Schurger et al. 2021; Brunia, Van Boxtel, and Böcker 2011).
During early development, it is believed that the brain makes use of its intrinsic rhythms to generate internal model(s) of the world by adapting to reflexive movements and homeostatic signals (Buzsáki, Peyrache, and Kubie 2014; Seth 2013). More generally, synchronization is posited as a fundamental mode of communication in the brain (Varela et al. 2001; Herbst and Landau 2016). A special case of synchronization is known as entrainment, where the temporal structure of an incoming stimuli modulates the brains intrinsic rhythms (Herbst and Landau 2016; Nobre and Van Ede 2018). Entrainment is usually seen in the lowest frequency ranges (0.1-4(7) Hz) in M/EEG recordings. In parallel to research conducted on rhythms of the brain from neurophysiological data, fMRI co-activations of brain regions have been increasingly modelled in terms of networks (Barabási et al. 2023). Recent work in theoretical network science has explored the properties of complex weighted networks (Böttcher and Porter 2024). Complex weights

means that the edges are characterized by complex numbers. As such, edges can encode information on both the real and the imaginary axis. Researchers have also showed that the concept of structural balance can be extended to complex weighted networks (Tian and Lambiotte 2023). In short, structural balance means that a network has a structure consisting of subgraphs that are internally integrated (strong positive internode relationships) and segregated (antagonistic relationships) between each other (see methods).

In this paper, we present an analysis that reveal whole-brain entrainment and anticipation in two fMRI motor task runs (381 subjects, Human Connectome Project, van Essen et al., 2012). Cortical and subcortical fMRI data was parcellated into 9 networks and 236 parcels (Schaefer et al., 2018, Fan et al., 2016). fMRI data was decomposed (empirical mode decomposition) into three intrinsic mode functions (IMFs) (99% of their power in [0.005-0.120], [0.011-0.3] and [0.021,0.684] Hz range, respectively) that together encompassed the entire sampling range up to the Nyquist frequency (0.7 Hz). We model brain activity as a series (time resolved) of complex weighted networks and introduce a novel phase clustering algorithm that divides the matrices into functionally meaningful components that are comparable across time.

We show that brain-wide patterns of entrainment to the task paradigm structure (visual cues, general block design) was present in the two slower frequency IMFs. Entrainment manifested as time-locked fluctuations in average community size as well as in parcel-specific synchronization across subjects. Task specific (hand, feet and tongue) cross subject phase synchronizations in association to movement was seen predominantly in the motor and somatosensory cortex prior to, during and after movement execution. Of note, synchronization started up to 12 seconds prior to task cue, which corresponded to a negative deflection in the averaged IMF3 timeseries, with its lowest point just before the cue. Parcels belonging to visual, dorsal and ventral attention networks, together with parcels located in the thalamus and basal ganglia, had more homogenous patterns of cross subject phase synchronizations. We interpret these motor specific and non-motor specific negative pre-cue deflections as the fMRI equivalent of RPs and CNVs found in M/EEG. In contrast to M/EEG, they were also present in single subject time-courses as reflected by the cross-subject synchronizations and were pervasive (in the case of CNVs) throughout most of the brain. Our results support the notion that anticipation have system wide effects on brain activity on the slow timescales of the BOLD-signal. It also gives support for that short term implicit learning of semi-complex paradigm structures help form specific expectations with high precision. From a theoretical standpoint, our results show that brain networks based on the IMFs fulfil the criteria of structural balance since the phase of any cycle will be 0. This also holds across time points. The phase clustering algorithm presented here is general in its applicability and can be used on any complex weighted network.

Methods

Data

Motor data

fMRI data from 381 young and healthy participants of both sexes from the HCP 1200 subject release were included in the study. The two block-related motor fMRI task runs (scanned back-to-back) used here was acquired right at the end of a close to one-hour long fMRI recording session. We will here refer to the first as run A (right-left phase-encoding direction) and the second as run B (left-right direction). We will here focus mostly on run B, but when appropriate, we will compare results between runs to highlight differences. The motor run included five types of movements (finger-tapping left, finger-tapping right, toe squeezing right, toe squeezing left, tongue movement Barch et al. 2013). The duration of each block was set to 12 seconds and was preceded with a 3 second cue. Each type of movement/block was repeated once. Additionally, three fixation blocks (duration: 15 seconds) were interspersed between motor task blocks.

The ordering of movements in runs A and B were different but some of the basic structure was preserved. Since the exact ordering of individual blocks in run A and B is important for the interpretation of the analysis, we would therefore refer the reader to Supplementary Figure 1 in which a detailed description is provided. Participants were given instructions of the task before the scanning began and then reminded right before the start of the task paradigm.

Preprocessing and parcellation

The minimally pre-processed volume-based data provided by the HCP was used, no further pre-processing of the data was conducted (Glasser et al. 2013). The pre-processing pipeline included gradient unwarping, motion correction in six directions, distortion correction using a field-map, non-linear registration to MNI- reference space using the FSL tool FNIRT and intensity normalization (Barch et al. 2013; Glasser et al. 2013). For cortical parcellation the Shaefer 200 brain area parcellation (7 Networks) was used (Schaefer et al., 2018). Additionally, the subcortical portion of the Human Brainnetome Atlas (Fan et al., 2016) was used to parcellate the thalamus, basal ganglia, hippocampus and amygdala. In total, the parcellation comprised 236 brain parcels. The parcellation of the amygdala and hippocampus were assigned to the “limbic network” in the Schaefer parcellation scheme while the thalamus and basal ganglia were treated as separate networks. The analysis therefore considered nine separate networks: Visual (VIS), Somato-motor (SOM), Dorsal attention (DAN), Ventral attention (VAN), Limbic (Limb), Frontoparietal (FPN), Default Mode (DMN), Thalamus (Thal), Basal Ganglia (BG). This was the same parcellation that we have used in previous works (Strindberg et al. 2021; Fransson and Strindberg 2023).

Complex weights, instantaneous phase and Empirical mode decomposition (EMD)

Time series data analysis is an example where complex numbers are ubiquitous. A real signal S can be represented in analytical (i.e. complex valued) form using polar coordinates $S = A \times e^{i\theta}$, where A is the amplitude of the signal, theta is the angle and i the imaginary unit. The same signal can be expressed in cartesian coordinates as $S = A(\cos(\theta) + i \times sin(\theta)$. The cosine term represents the real part of the phase angle, and the sin component represent the imaginary part.

Signal phase is one of the classic measures to assess co-activation between regions of the brain (Varela et al. 2001; Glerean et al. 2012). It has mostly been used in MEG and EEG studies but also to some extent in fMRI data analysis (Glerean et al. 2012; Cabral et al. 2017; Strindberg et al. 2021; Niazy et al. 2011; Ponce-Alvarez et al. 2015; Fransson and Strindberg 2023). Phase synchronization is the alignment of phase of two signals. It can refer to the relationships between two signal time series across time, where in the idealized case the phase between the two timeseries are fixed. It can also refer to a single timepoint by estimating instantaneous phase using the Hilbert transformation (Honari, Choe, and Lindquist 2021). The assumption is that a small difference in phase translates to information exchange between regions (Varela et al. 2001). Thus, the smaller the difference the stronger the cooperation. An important methodological strength of phase as a measure of interregional relationships in the brain is that it quantifies relationships on a continuous spectrum of positive and negative values. This is conceptually similar to correlation that also span the positive and negative dimensions, but with the added advantage of being time resolved in the case of instantaneous phase. Previous studies have shown a high similarity between measures using time-resolved phase information and Pearson's correlation when assessing pairwise relationships between (Strindberg et al. 2021).
Importantly, the instantaneous phase extracted with the Hilbert transform must be unambiguous. This implies that the timeseries cannot contain riding waves, which is usually present in real world signals. The most common approach to make time series unambiguous is the usage of narrow band pass filtering. However, narrow band filtering means that a lot of information in the signal is lost. It also means that arbitrary cut-off frequencies for the filter must be set. It remains an open question which frequency range of the BOLD-signal that contains neuronally associated information. Some argue for a very narrow range while there is also evidence pointing to a wide range of meaningful frequencies within the BOLD-spectrum (Niazy et al. 2011).

Taken these factors into consideration, we opted to use the empirical mode decomposition (EMD) algorithm. The EMD is a data driven alternative to narrow band pass filtering to get time series without riding waves (Huang et al. 1998). The EMD is a heuristic algorithm that decomposes a timeseries into its intrinsic mode functions (IMFs). The EMD does not require any assumptions regarding stationarity, linearity or frequency range. It's a heuristic sifting algorithm that aims to extract oscillatory modes from the timeseries such that the total number of maxima and zero crossings differ by at the most one. This means that there will be no riding waves and no ambiguity regarding the phase. In addition, the waveforms are locally approximately symmetric (Huang et al. 1998). The IMFs contains frequencies in falling order such that the first IMF contains the highest frequencies and the last the lowest. There are no sharp boundaries in frequency content between IMFs. BOLD signal time-series from all parcels, runs and subjects were

decomposable to at least three IMFs. Therefore, we report results from all three with a focus on third IMF (IMF3), which power spectrum most closely reflect the classical 0.01-0.1 Hz spectrum considered in fMRI data analysis.

Phase clustering algorithm

As a starting point, we consider the instantaneous phase difference between all parcels at each time point *t*, by defining the dense complex weighted matrix M_t. Dense means that all edges are included with thresholding. Each entry $M_t(x, y)$ is an edge that describes the instantaneous phase difference $\theta_{x,y}$ between parcel (node) x and y at time t. The algorithm is greedy and has a hierarchical structure. It optimizes for two main criteria: integration (criteria one) and segregation (criteria two). Integration here means that *all* pairwise relationships within the same community have maximum phase difference defined by threshold one, $thr1 = \cos(\theta_1)$. We investigated six different choices for θ_1: $\frac{\pi}{2}, \frac{\pi}{3}, \frac{\pi}{4}, \frac{\pi}{6}, \frac{\pi}{9}, \frac{\pi}{18}$. The community is *phase consistent* at the chosen threshold. Segregated means that *all* pairwise relationships between nodes in two opposing communities have a *minimum phase difference* defined by threshold two, $thr2 = \cos(\theta_2)$, where $\theta_2 = \frac{2\pi}{3}$. There are also two secondary, more generous thresholds, to account for scenarios where lesser degrees of segregation are present: $thr2b = \cos(\theta_{2b})$, where $\theta_{2b} = \frac{\pi}{2}$ and $thr2c = thr1$. $Thr2b$ is only relevant in situations where no cluster is formed based on $thr2$ and $thr2c$ only when non is based on $thr2b$. A scenario where $thr2c$ is not enough is equal to one single phase consistent cluster based on $thr1$. Each iteration, the algorithm aims to identify a pair of maximally segregated (criteria two), phase consistent (integrated) communities (criteria one) if a minimum segregation of at least $Thr2c$ $(= thr1)$ exists in the data. In the first iteration, to harmonize communities across timepoints, the first community is based on the parcel with the smallest instantaneous phase value, i.e. - π in the idealized case. The second community is then defined based on the parcel most segregated with the seed parcel of the first community. In subsequent iterations, the starting point is the identification of the nodes with the strongest phase relationships (positive, negative and both). These nodes form the first tentative cluster. If this group of nodes also turn out to be integrated (criteria 1, $thr1$), they form the first community. If the group is not integrated (violates criteria 1), subcommunities are investigated to find the largest subcluster that is integrated.

As for the first iteration, the second community is defined based on maximizing criteria 2 while fulfilling criteria 1. Communities formed beyond the first iteration are sorted based on their leading and lagging relations to the communities in the first iteration. The imaginary component (*sin)* of the phase difference between two communities provides information of which community is leading, and which is lagging.

Let ϑ_1 be instantaneous phase of Com1 and ϑ_2 that of ComX. Then, if $\sin(\vartheta_x - \vartheta_1) > 0$, Com X is leading in relation to Com1. However, this is a truth with modification since $\vartheta_1 = \vartheta_1 + 2\pi$ in which case Com1 would be ahead of Com X. If a leading community already exists, a secondary leading community will be formed. If instead $\sin(\vartheta_x - \vartheta_1) < 0$, Com X would be lagging in relation to Com 1.

We present the results of $\theta_1 = \frac{\pi}{3}$ in the main text, a summary of the other results is found in the supplement. The algorithm is designed for community comparison between multiple iterations of a complex weighted network where the distribution of phases is

assumed to be similar across iterations. In the case of timeseries, the iterations are discrete timepoints. The algorithm can be adapted to situations where distribution of phase varies widely between iteration. This is done by using the iteration with the largest distribution as reference.

Structural balance

The theory of structural balance originated from psychology and got its mathematical formalization in the 1940's and 1950's (Harary 1953; Cartwright and Harary 1956). Structural balance originally refers to the overall organisation of signed networks with both positive- and negative-valued edges (Zaslavsky 1982). This contrasts with most graph theoretical renderings of brain data that largely focus exclusively on positive weights. The notion of balance is defined through cycles in the network, i.e., paths that start and end at the same node. A signed network is said to be balanced if all cycles in the network contain an even number of negative edges (Harary 1953). In the extension to complex weighted networks, a network is structurally balanced if all cycles satisfy the condition that the sum of the phases of all edges in the cycle is multiples of $\frac{\pi}{2}$, or the phase of the cycle is 0 (Tian and Lambiotte 2023). Instantaneous phase of a set of smooth time series is a special case of a sequence of complex weighted networks. For this case, the concept of structural balance can be extended across time since the realization of paths will be limited to progression of phase for any node.

Phase shuffled data

To test that the results were not merely driven by chance, we applied the algorithm on surrogate data. Since the key property of investigation was phase, we used phase shuffled data as our surrogate (Lancaster et al. 2018). Shuffling of the phases preserves the power spectrum of a time course while destroying the temporal order of phase. To this end we shuffled the phase of the bold time series of run B. Due to edge effects resulting from the phase shuffling process, 20 time points were excluded at the beginning and at the end of each timeseries instead of only 10 which were excluded in the real data.

Results

Community division

The phase clustering algorithm was designed to create communities that spanned a limited phase range in a reproducible way. This means that as edge weights in a community change in different renditions of a network (e.g. across time), community numbers will always reflect a similar phase range. We investigated six different thresholds (θ_1) for phase consistent communities. By design, for a matrix that contain the full phase range $[-\pi, \pi]$, the algorithm will create a post-nadir and a post-peak community. The space between them is then systematically divied into four sections that are increasingly subdivided as θ_1 get smaller. For small θ_1 ($> \frac{\pi}{2}$), beyond the first iteration, each iteration creates communities largely spanning the intersection of the preceding two iterations. With diminishing θ_1, the relative size of the post-nadir and post-peak communities gets smaller. The result, independent of θ_1, is communities which forms are mirror images of

each other such that $[0, \pi/2]$ mirrors $[\pi/2, \pi]$, $[-\pi/2, 0]$ mirrors $[-\pi, -\pi/2]$ and $[0, -\pi]$ mirrors $[-\pi, \pi]$ (Fig. 1). Similar results will be found for all complex weighted matrices that spann the range $[-\pi, \pi]$ (See supplement on phase scrambled and random data).

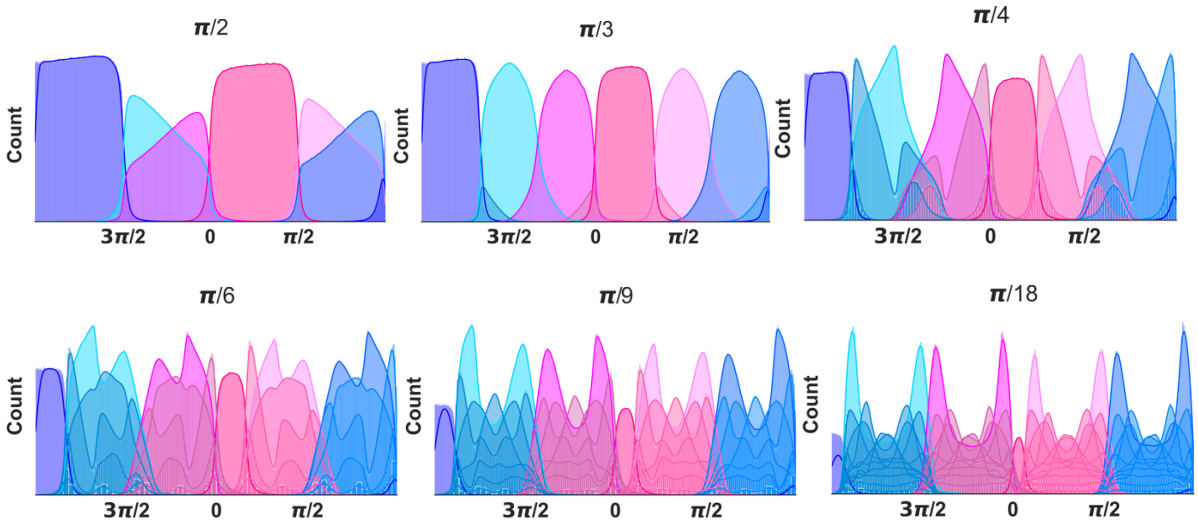

Fig 1. Motor task data (Run B). Phase (in radians) distribution (across subject, parcels and timepoints) per community (plot is cut between $[\pi, -\pi]$) for different $\boldsymbol{\theta_1}$: $a)\ \frac{\pi}{2}, C = 6,\ b)\ \frac{\pi}{3},\ C = 10,\ c)\ \frac{\pi}{4}, C = 14,\ d)\ \frac{\pi}{6}, C = 22,\ e)\ \frac{\pi}{9}, C = 30,\ f) \frac{\pi}{18}, C = 45$. Cluster colour beyond $C = 10$ are a reptation of colours for $C\ 7 - 10$.

Progressive community switching

We defined a community switching matrix to answers the following question: ***If*** a parcel is found in Com X at time *t*, what is the probability that it will ***switch*** to Com Y at time *t+1* (X and Y can be the same parcel, i.e. X =Y)? The sum of all elements in the switching matrix with this definition is equal to one. This means that the probability is a count of the switching per see and not the probability to be somewhere. However, the probability to be somewhere is the sum of all the switches. Note that this is not the same as the classical switching matrix where each row sums to one. Instances were calculated cumulatively, and the sum was divided by the total number of time points, then average was calculated across subjects. The resulting number is the probability or dwell time. Given that the phase cluster algorithm was constructed to capture phase consistent communities, it was expected that community switching from the point of view of the parcels (nodes) followed the progression of phase and its associated community. This was indeed the case independent of θ_1 (for illustrations of the switching matrix for all thresholds see Suppl. Fig. S2).

Structural balance

Given that the data could be clustered as phase consistent communities, any cycle will have phase = 0. Thus, the criterium for structural balance is fulfilled. Importantly, when the complex weights represent smooth time series, the criterium for structural balance is fulfilled also across time as shown by the switching matrix; all actualized paths of nodes

will follow the progression of phase. This means that they will return to the community of the starting point, thus the phase of such a cycle will be zero.

Cross-subject synchronization

In the following we will present results for of $\theta_1 = \frac{\pi}{3}$ (A short summary of the results for of $\theta_1 = \frac{\pi}{2}$ can be found in the supplement, Suppl. Fig S19-22) applied to the fMRI motor task data. It resulted in six major and four minor communities (for brevity, named COMs, Figures 1b, 2a). The major communities were close to equal in size, and each spanned a limited section of the unit circle with only minor overlap. Major communities were numbered in order as they appeared on the unit circle where COM1 was the post-peak and COM4 the post-nadir communities. The minor communities spanned the intersection between COM1 and COM2 (COM7), COM3 and COM4 (COM8), COM4 and COM5 (COM9) and COM6 and COM1 (COM10). Moreover, the minor communities had a preferential switching probability pattern same as of one the intersecting communities. COM7 could therefore be considered a minor community of COM1, COM8 of COM3, COM9 of COM4 and COM10 of COM6. The relative size (proportion of parcels) of the six major communities was close to the theoretical mean (1/6) 0.160 [range: 0.150,0.175]. The minor communities were substantially smaller (mean size 0.0118 [range: 0.011,0.013]). The six major communities were (except for a few time-points) present in the data at all timepoints for all runs and subjects. Up to three additional communities were present in 23% of subjects. However, these were exceptions to the community results presented in Figure 1, and together they represented only 0.3% of the data points and were disregarded in the subsequent analysis. Very similar results were seen for the other IMFs and in run B.

The analysis revealed two types of task-locked synchronizations across subjects. The first was a highly regular, close to oscillatory, fluctuations in average community size, observed in all communities. Size-related fluctuations were time locked to the task paradigm independent of which specific motor task that was performed. The oscillatory peaks followed the switching order of the corresponding communities, i.e. the progression of phase (Figure 1, Suppl. Fig S8a, b). Thus, COM4, the post-nadir community, peaked at each cue (and at the time-point where the cue would have been for the fixation blocks). The remaining five major communities peaked in a progressive order such that all had a peak within a 15 s of cue+ task period, thus completing a cycle (see Suppl. Fig S8 c, d for a sorted presentation of positive deflection and negative deflection communities respectively).

.

The second type was a parcel specific pattern of phase synchronization across subjects in relation to the timing of the motor task. Common patterns were seen within the canonical resting-state networks (RSNs), but many aspects were also shared between RSNs. As can be seen in Fig 2, the task paradigm induced brain wide cross subject phase synchronization across communities. It was most pronounced in the visual, attention (DAN, VAN) and somato-motor networks, particularly the motor movement specific parcels. The limbic and default mode networks showed relatively low levels of

synchronization. A more detailed account of the parcel specific synchronizations will be given in the section on parcel specific synchronizations below.

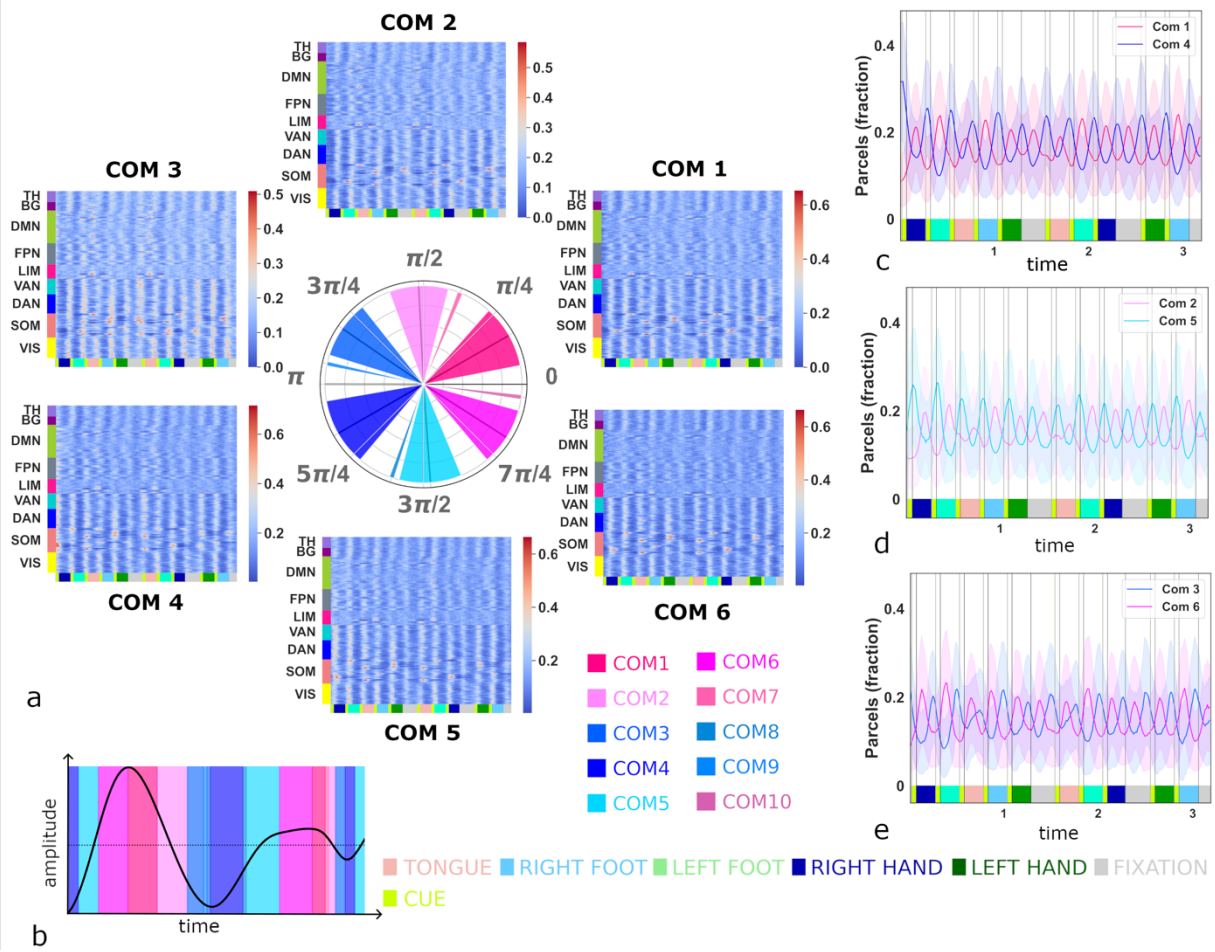

Figure 2. Summary of the relationships between the common six major and four minor communities computed from fMRI motor data ($\theta = \frac{\pi}{3}$ $, run\ A$). **(a)** Communities plotted on the unit circle according to phase distribution (radians). Each community wedge is centred at its mean value and its width is defined to be 2 standard deviations (2 SD). The six large wedges in the unit circle correspond to the major communities (COM 1-6) and thin wedges correspond to the four minor communities. The unit circle is surrounded by the community specific synchronization plots displaying all parcels sorted by network (COM 7-10, see Suppl. Fig S4). An example (cut time-series of motor parcel) of the change of community according to phase is given in panel (**b**). Panels (**c, d,** and **f**) shows the average (across subjects) size of communities (fraction of the total number of parcels) as a function of time for the six major communities (see also Suppl. Fig S8). Communities are plotted in pairs of maximum segregation (opposite sides of unit circle). Grey lines indicate start of cue; black lines indicate start of task/fixation period in panels (**c, d** and **e).**

Parcel and network specific cross-subject phase synchronizations

Next, we took a closer look at parcel specific cross-subject phase synchronizations. It was defined parcel-wise as the fraction of subjects with same community assignment at the same time. We summarize some general findings. We also describe the specific synchronization patterns of the key parcels related to motor movement located in the motor and somatosensory cortices (see Figure 3). Finally, we look at some specifics of the visual, dorsal and ventral attention network synchronizations.

Parcel specific synchronizations were seen in IMF2 and IMF3 but not in IMF1. In both IMF2 and IMF3, synchronizations were time locked to task blocks and involved all regions of the brain to some extent, with the exceptions of some sections of the amygdala, hippocampus and thalamic nuclei. In IMF2, which spanned a higher frequency range with a peak at 0.1 H, synchronizations were present but with relatively low amplitudes (For further results on IMF2 see section "IMF2 results" in the Supplement, Suppl. Fig S11). Amplitudes and durations were higher in IMF 3 (peak 0.03 Hz) reflecting the slower frequencies (See Suppl. Fig S3). Some common patterns of were shared among most parcels. Degree of synchronization fluctuated for most parcels across time. The synchronization of the post-nadir community (COM4) peaked right before or during the cue. A cycle (i.e. sum of phase shift = 0) of synchronizations was completed during the 15s of task + cue in the same way as for average community size oscillations. Notable exceptions to this general pattern were the motor movement specific parcels in motor cortex and some somatosensory parcels, some parcels of the OFC, temporal pole and a single DAN parcel.

Strongest peak synchronizations were seen in the hand somatosensory cortex corresponding to the first block of hands movements. Generally, the synchronizations of the motor cortex were highly specific for each motor movement. The tongue movements induced close to equal size synchronization in its associated motor regions in both hemispheres. Hand activations were unilateral while the feet motor parcels showed a weak synchronization also when the contralateral foot moved. The synchronization pattern changed prior to and during the movement specific to each motor parcel. Synchronization was then more pronounced, with higher amplitudes and longer period and duration (reflecting a slower and larger amplitude average IMF3 waveform). Pre-cue synchronization also started earlier, approximately 12-15 s *before* the task specific cue. The degree of synchronization increased gradually reflecting a progressively larger number of subjects with the time course in the same phase. Pre-cue synchronization was maximal right at or during the cue, corresponding to the post-nadir community and a deflection in the average IMF3 time course. Given the time-locked fluctuations in community size described earlier (Fig 2c-e), this implied a maximal segregation with the parcel(s) responsible for the execution of the immediately preceding task at this time. In other words, the phase of the parcels that were synchronized during the preceding motor task block were now maximally segregated with respect to the phase of the community of parcels being synced during the next task.

Peak activation was close to the end of the task (Fig 3). Motor task specific activations lasted in general approx. 42 s, i.e. 12 s before (preceding task + cue of current task) and 30s (current task + subsequent cue and task + cue of second next task) after the cue translate to approximately 1.5 cycles (where the sum of phase shift of one cycle = 0). Even

though the pre-cue synchronization preceding each task-block was specific to each motor task in their corresponding motor and somatosensory parcels, there were also smaller but visible patterns of much more attenuated synchronization prior to most task block. This pattern was more pronounced in two of the somato-sensory parcels in the right hemisphere associated with the left hand and left inferior inter-effector (IE) parcels (see separate results of IEs below). For results on IMF2, see Supplement.

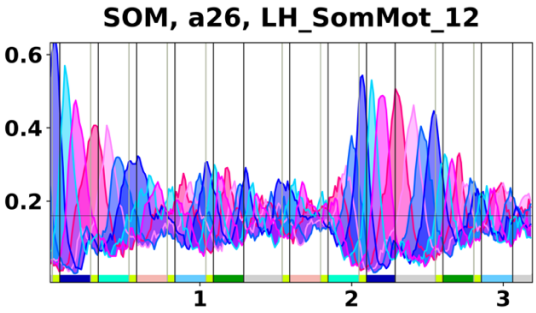

a. Right hand motor

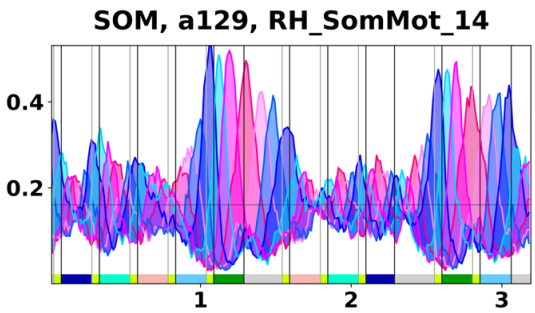

b. Left hand motor

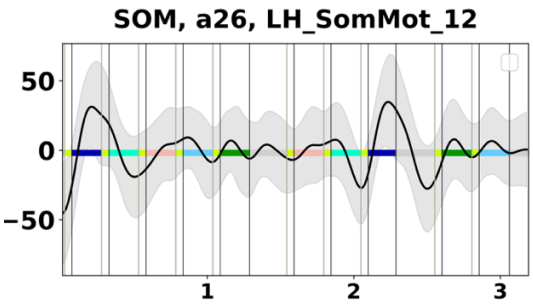

b. Right hand motor

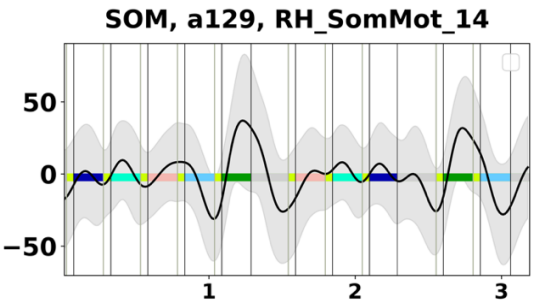

d. Left hand motor

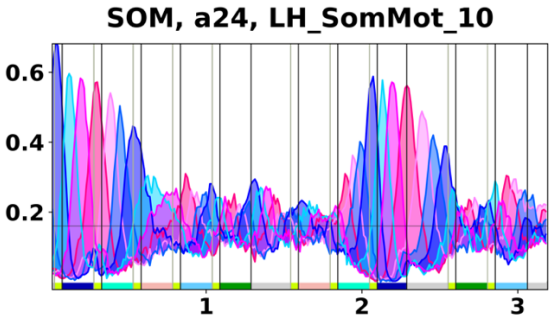

e. Right hand somato-sensory.

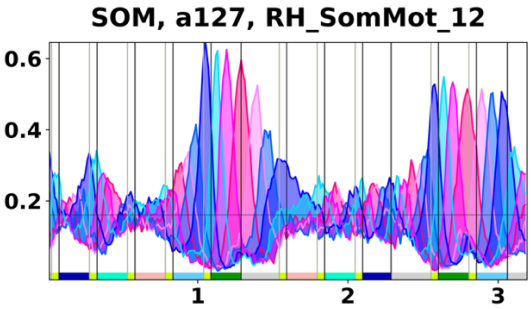

f. Left hand somato-sensory

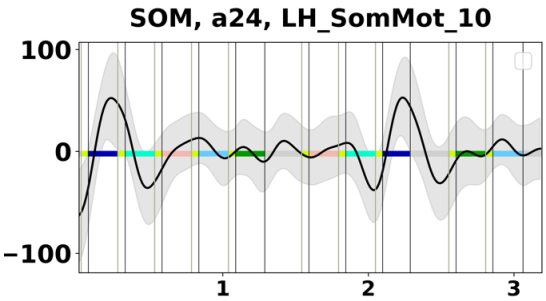

g. Right hand somato-sensory

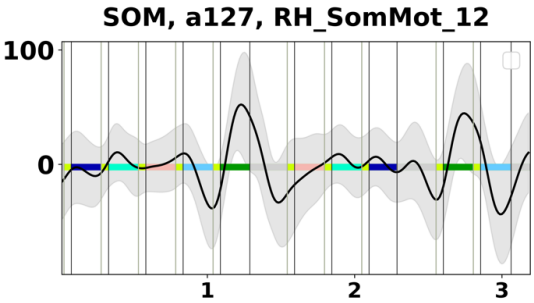

h. Left hand somato-sensory

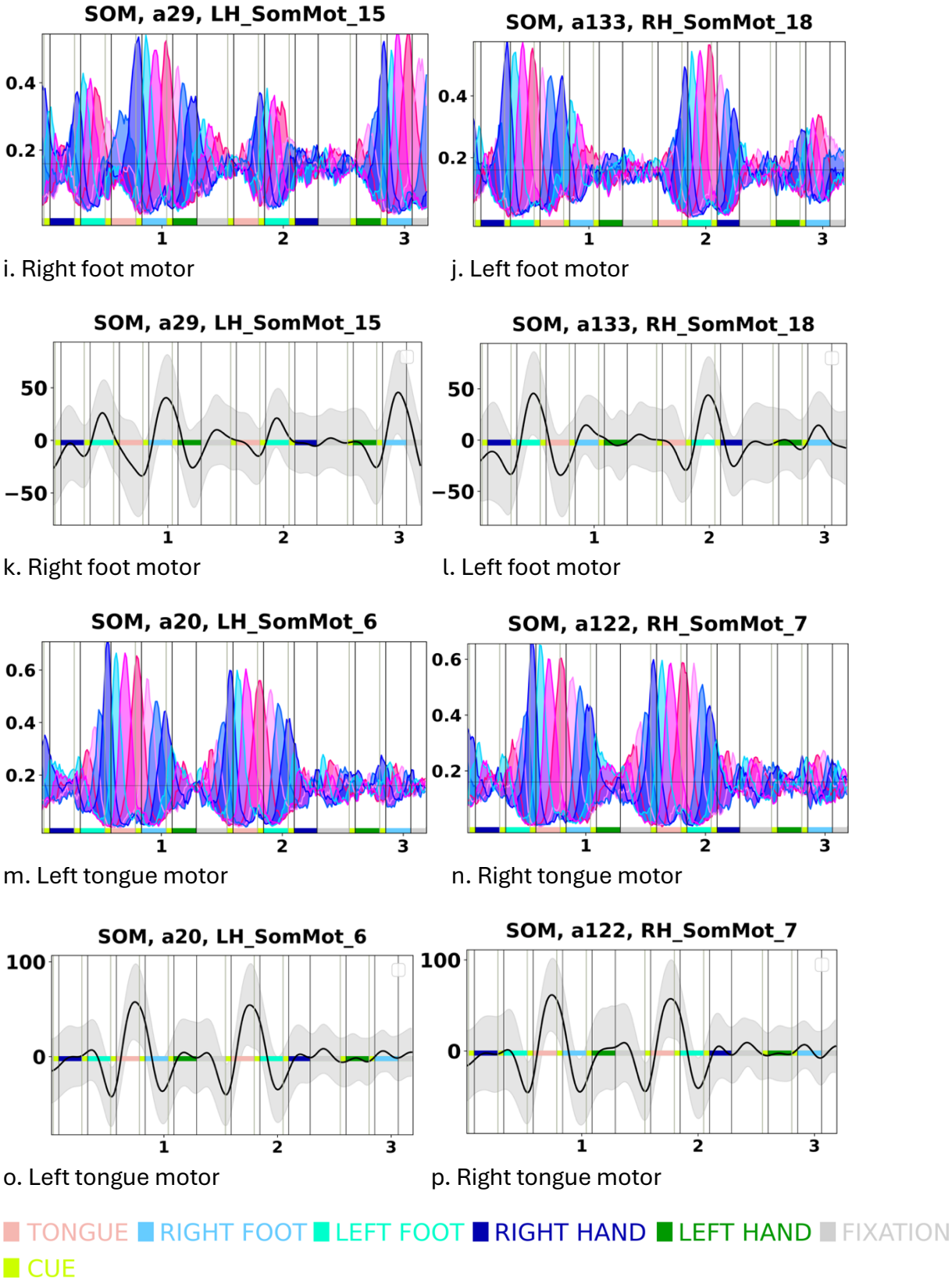

Figure 3. Synchronization timeseries and mean (IMF3) timeseries (SD=grey shadows) for the six motor parcels and the two somatosensory parcels with strongest synchronization (Run B). Horizontal line at the random mean of community assignment 0.16 (fraction of subjects) The mean IMF time series are placed right under the corresponding synchronization time series. **a)** Right hand motor (a26), **b)** Left hand motor (a129), **e)** Right

hand somatosensory (a24), **f)** Left hand somatosensory (a127) **i)** Right foot motor (a29), **j)** Left foot motor (a133), **m)** Right Tongue (a20), n**)** Left tongue (a122). Dark blue = Right Hand, Light Blue = Right Foot, Dark Green = Left Hand, Light green = Left Foot, Peach = Tongue, Grey = Fixation, Lime = Cue. (Headings reflect the names of the Schaefer Parcellation and will be removed in an updated version.) For results for Run A see Suppl. Fig S9 and S10.

Synchronization episode participation

We also calculated the participation rate during each episode of synchronization for IMF 3. This provided a fuller picture of the synchronizations of subjects by considering some of the variability in timing. While the amplitudes of the cross-subject synchronization time-series accounted for the fraction of subjects that synchronized at any given time point, the participation rate accounts for the fraction of subject that contribute to the amplitude during periods when it reaches above the baseline. An episode of synchronization was defined as at least two consecutive time points above the baseline synchronization (0.16). Participation in the synchronization episode was defined as synchronizing during at least one timepoint. Calculation was done separately for each of the six community synchronization timeseries. Average participation rate was calculated across synchronization episodes for each community. Average was subsequently calculated for each parcel across communities (Fig. 4d, e). Fewer episodes of synchronization were associated with higher participation rates for most parcels (Pearson's r=0.80), mainly due to longer duration. For the six motor parcels, the average maximum participation rate across the six first communities were 0.92 (SD 0.02, range [0.9,1]). This meant that in principle, almost all subjects were part of the synchronization episodes of the parcel specific movements. However, the calculation was an underestimation since it did not consider the full extent of the area below the curve (i.e. section below average). As is seen in Figure 2, a peak in synchronization was usually followed by a sharp reduction of synchronization.

Phase synchronization associated to movements of the tongue.

The tongue movements elicited segregated (anti-phase) synchronizations as well as some leading and lagging synchronizations in the temporal pole, orbitofrontal (OFC) and ventromedial prefrontal cortex (vmPFC), in parts of the basal ganglia (middle and ventral sections of caudate nucleus, lateral aspect of lentiform nucleus) and in a single parcel of the DAN(a137). These synchronizations had the same extended synchronization periods as the motor parcels reflecting slower and larger IMF waveforms. The patterns where also partly opposite in the two runs (what had been anti-phase in one was in-phase in the other) and was more extensive in the second run. The strength in terms of max synchronization varied between parcels and was weakest in the parietal cortex and basal ganglia (See Suppl. Fig S12 for illustrates of the tongue associated synchronizations for the two runs). See Supplement for IMF2 results.

Visual network (VIS)

The visual network showed in general a sustained synchronization pattern that was time locked to each task block with nadir right before or at cue (Fig 4b1.1). Most of the VIS parcels desynchronized during fixation periods. For many of these parcels, the pre-cue nadir was less pronounced. After the nadir, the synchronization pattern broke down during the period of the fixation block. For many of the parcels, the pre-cue synchronization prior to the subsequent task was absent (See Fig 4b1.1). In run B, for some of the parcels, there was a dip in synchronization at the place where the first fixation period was placed in Run A (See Suppl. Fig S13).

Dorsal attention network (DAN)

The parietal cortex right behind the somatosensory cortex belongs to the DAN according to the Schaefer parcellation. These parcels showed motor movement specific synchronizations. The most medial parcels (behind the feet somatosensory cortex, parcel 40 and 144) showed synchronizations with both feet and to a lesser extent with the ipsilateral hand (It also had a negative peak right before the two first fixations). The medial parcels of the DAN along the posterior midline showed similar patterns with synchronizations with the feet and ipsilateral hand. They showed no synchronizations with the tongue movements or the contralateral hand. The DAN parcel behind the tongue motor parcels synchronized with tongue and hand movements bilaterally but not with feet or fixation. Of these, one parcel hade the same protracted synchronization pattern as the motor and somatosensory parcels (a137). The DAN parcels located behind the hand somatosensory cortex also mostly synchronized with hands and tongue.

Ventral attention (VAN)

Activity in motor cortex is proceeded by activation of the supplementary motor cortex (SMA) and pre-SMA (Gordon et al. 2023). In neurophysiological recording, the RP is mainly seen over the SMA and pre-SMA. In the Schaefer parcellation used here the SMA is part of the ventral attention network (VAN) attesting to its involvement also in attentional processes (Schaefer et al. 2014; Travers, Friedemann, and Haggard 2021). In our analysis we found that bilateral SMA, right precentral sulcus, left inferior precentral sulcus and right supramarginal gyrus (SMG) showed a particular synchronization pattern (Fig. 4b); Sync was highest at the start of the run and tapered of gradually, then increased again at the end of each fixation block to taper of afterwards (Fig 4c). The SMA parcels cross-subject synchronization timeseries were almost perfectly correlated (r=0.994). SMA cross-subject synchronization timeseries had highest correlation with pre-SMA, dACC, SMG, anterior insula, dorsolateral prefrontal cortex (dlPFC)(Fig 4a). These are the same regions that are known as the cingulo-opercular network or timing network in different contexts (D'Andrea et al. 2023; Bader and Wiener 2023).

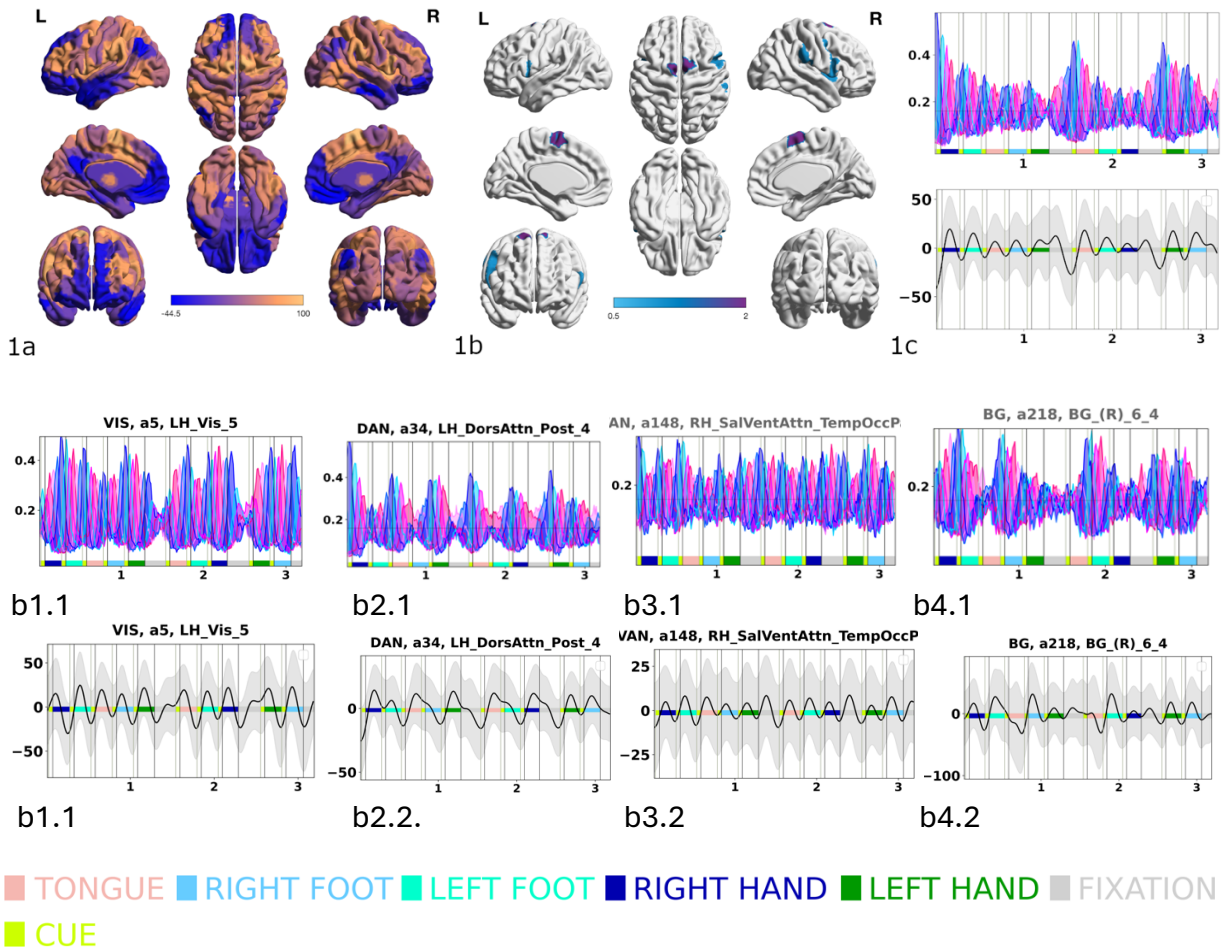

Figure 4A. **1a)** Synchronization timeseries correlation for SMA (a158) with the rest of the brain shows the Cingulo-opercular network (CON) also refered to as the Timing Network (TN). **1b)** Subregions of CON with increased synchronization during higher levels of anticipation. **1c)** Synchronization timeseries of right SMA and corresponding average IMF3. **4B**. Example of principally different synchronization patterns (Run B). bX.1 = cross-subject synchronization time series, bX.2 average IMF3 time series**.** **b1)** Visual parcels that show desynchronization during fixation **b2)** DAN parcel that synchronizes on every second task. **b3)** Uniform/sustained synchronization of VAN parcel **b4)** Uniform/sustained synchronization of VAN parcel. B6 Synchronization of a BG parcel. See Suppl. Fig S11 for IMF2-equivalents of b1-4.

Synchronization correlation across the brain

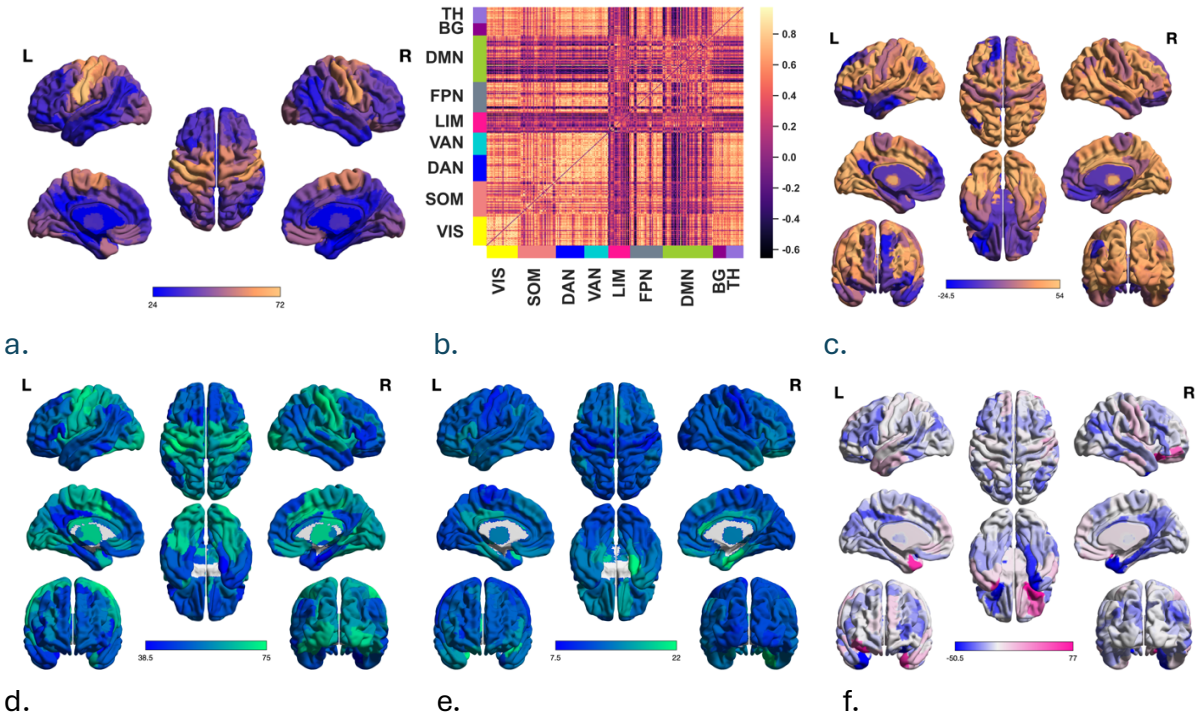

Figure 5. a) Max synchronization (run B, see Suppl. Fig S14 for run A) Highest levels of synchronizations were seen in motor cortex, somato-sensory cortex and SMA. **b)** Pearson's correlation between synchronization timeseries, average between six main communities. **c)** Synchronization correlation matrix mean per parcel plotted on the brain for clarity. Correlation matrixes were computed for each of the six first synchronization timeseries then averaged across the six. DMN and left limbic parcels had lower averages in the left hemisphere compared to the right. **d)** Average number of subjects that synchronized during an episode of synchronization. A period of synchronization was defined as minimum of two consecutive timepoints above the baseline, i.e. theoretical mean 0.16 (=1/6). The somatosensory cortex of the right hand showed the highest participation rate during above baseline synchronization periods (75% of subjects). DMN and some of the FPN show lowest level of synchronization participation **e)** Average number of above baseline synchronization periods. The pattern was mostly the opposite to that in a) such that parcels with high participation had fewer (and longer) episodes of synchronization. Right cingulum, PCC and OFC show highest rates also reflected for most part in low average levels of synchronization participation both at single time points and synchronization episodes. **f)** Change in synchronization between runs.
Footnote: amygdala, hippocampus, basal ganglia are not shown

Peak synchronization reflected the maximum cross-subject synchronization for each parcel across time and communities (Fig 5a). Highest levels of synchronizations were seen in motor cortex, somato-sensory cortex and SMA. To understand to what extent synchronization timeseries were similar beyond periods of peak synchronization, Pearson's correlation coefficient was calculated between synchronization timeseries for pairwise parcels. The correlation coefficient was then averaged over the six main

communities to get an average correlation (Fig. 5b). The attention networks (DAN, VAN) as well as VIS, BG and Thal showed relatively high average correlations and low variability among parcels: VIS (r=0.45, sd = 0.06), DAN (r =0.46, sd 0.06), VAN (r = 0.45, sd =0.05), BG (r=0.42, sd=0.05) and Thal (r = 0.45, sd =0.04). The Limbic Network (r =.11, sd = 0.17) and DMN (r = 0.19, sd = 0.20) had the most negative correlations and hence a lower average correlation. The FPN (r =0.4, sd = 0.18) was also more heterogeneous. The six main motor parcels showed relative low average correlation with little variability (r=0.20, sd =0.02) while the SOM as whole was more heterogeneous (r= 0.36, sd =0.11). The similarity with Run A was high (r = 0.86 between runs), but with some important differences. The first run had more strong negative correlations, while the B run had more strong positive correlations. The largest difference between the two runs was seen for parcels belonging to the DMN and Limbic networks that responded specifically to tongue movements (Suppl. Fig S12).

Synchronization correlation for each of the six principal motor parcels

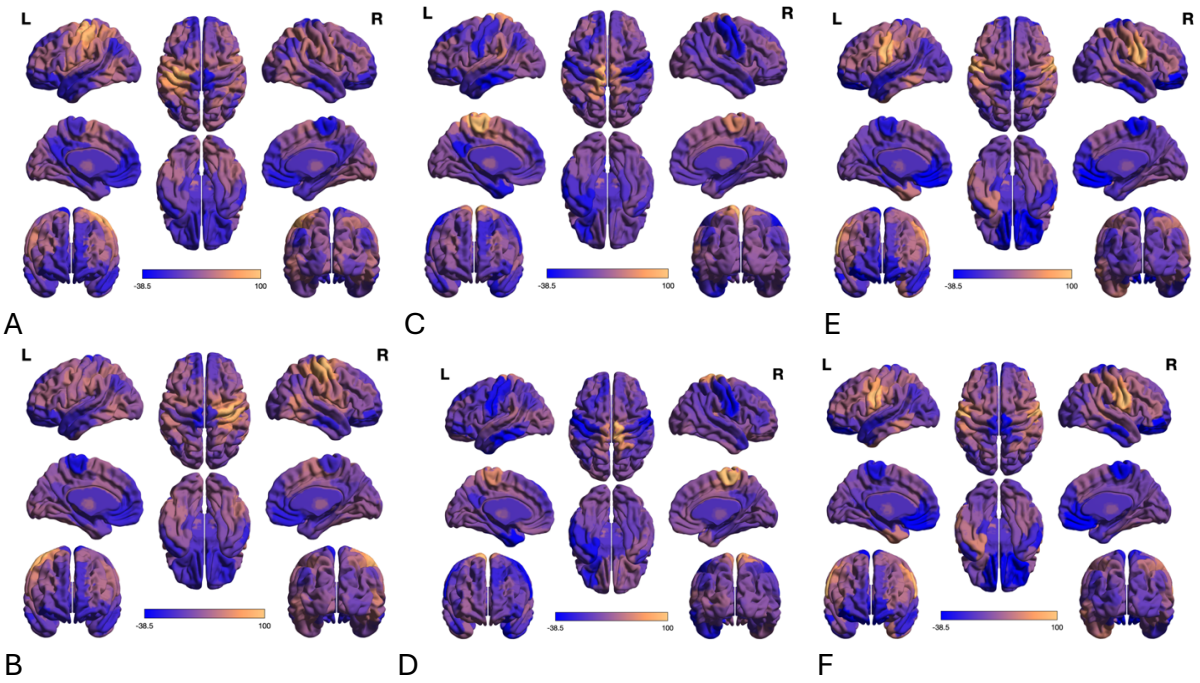

Figure 6. Average correlation between synchronization timeseries for each of the six motor parcels. The mean is taken across the six community synchronization timeseries, same as in figure 4. In each plot, the motor parcel has correlation value 1. Plots are normalized to the lowest correlation across the six parcels for easier comparison. A) Right hand, B) Left hand, C) Right foot, D) Left foot) E) Tongue (left hemisphere), F) Tongue (right hemisphere)

The hands regions of the motor cortex showed strongest positive correlations with their respective somatosensory regions (r range 0.91,93]) as well as the parietal regions right

behind the post-central gyrus belonging to the DAN (r=0.74 for both hands). The strongest anti-synchronizations were seen with the motor and somatosensory regions of the contralateral foot (r range [-0.25, -0.26]) while no correlation was present with the ipsilateral foot. Both hands were mostly decoupled from DMN , LN, FPN, Thal and BG but with relative high average correlation with DAN (RH r=0.45, LH r=0.44), and VAN (RH r=0.40, LH r=0.39) as well as large parts of the SOM (r = 0.29) except the feet, BG (RH r=0.29, LH r 0.30), Thal (RH r=27, LH r=0.32).

The left foot had highest correlation with its somatosensory parcel (r=.93). Right foot motor parcel was merged with its somatosensory parcel. Correlation between feet r=.61. Both feet had relatively high correlation with the ipsilateral DAN (r range [62,67].) The feet had higher correlations with the BG (RH r=0.39, LH r 0.35) than the hands. Correlation with Thal (RH r=37, LH r=0.31) was like that of the hands. Strongest anticorrelation was seen with the tongue for left foot (r=-.35) and with the contralateral middle IE for the right foot (r=-0.33). For the rest, the feet showed low degrees of correlation in synchronization timeseries.

The average correlation of the synchronization timeseries of the two motor parcels controlling tongue movement was very high (r=.97). The tongue motor parcels were also strongly correlated with the parietal cortex right posterior to the tongue somatosensory cortex. DAN (a137) r=0.83, a138 r=0.52, a139 r=0.5. Neg correlation with feet and parcels of the OFC (Limbic Network) and vmPFC and frontal poles (DMN).

Inter-effector regions (a18, a21, a120, a125)

Recently, the traditional somatotropic organization of the motor cortex that divides it into sequential motor regions ("the homunculus") have been called into question. New evidence suggests instead that the motor cortex is organized in three concentric effector regions per hemisphere (regions responsible for more fine grained movement are located at the centre and more coarse movement at the periphery) responsible for motor actions (Gordon et al. 2023). The effector regions are interspersed with three inter-effector (IE) regions. The IE regions are highly connected to each other and the cingulo-opercular network (CON). The inter-effector regions are proposed to be responsible for whole body integration and motor planning and show non-preferential activation with motor movement. The original study describing the IE regions was done on highly sampled individuals, but the inter-effector regions was also found to be present in the group average of the three to date largest open-source datasets (Gordon et al. 2023).

In the Schaefer 200 area parcellation used in this study, only the equivalent of the middle and inferior IE regions can be identified i.e. the parcels lateral to the tongue and between tongue and hand motor regions. In line with the results described above, we found that the synchronization timeseries of the IEs were generally strongly correlated with each other (bilateral inferior IEs most pronounced, r=0.91) except for the left inferior IE and right middle IE (r=0.57). In contrast to the results from the Gordon study that investigated single subjects, the IEs did show a preference for specific motor activity in that they synchronized more with tongue and hand movements than the feet. Average correlation synchronizations timeseries revealed an overall weak or negative association between

the IEs and the feet (Pearsons' r range [-0.33,0.21], ipsi- and contralateral relations)), bilaterally generally strong correlations with the tongue (Pearsons' r range [0.69,0.78], ipsi- and contralateral relations) and the hands (Pearsons' r range [0.34,0.85], ipsi- and contralateral relations) with a preference for the ipsilateral side.
In contrast to the original study, only the average synchronization timeseries of the inferior IEs had positive correlations with the cingulo-opercular network (dACC, SMA, supramarginal gyrus (Brodmann area 39), middle and anterior insula) (Suppl. Fig S15). There were also widespread strong correlations with the dorsolateral PFC and Brodmann area 37 bilaterally. There was a notable increase in synchronization of right hemisphere IEs in the second run (B) compared to the first (A). Both parcels also showed a stronger preference for tongue movement in the second run (Suppl. Fig S16-17). Right hemispheric IEs also had a more temporally extended synchronization pattern like that of the motor parcels.

Comparing motor task run A and run B

We compared level of synchronization between the two runs for each parcel by integrating the common envelope of cross-subject synchronization timeseries. This was done by summing the difference between maximum and minimum synchronization at each time point. The relative change was calculated as the difference between the sums of two runs divided by the sum of the first run. Positive values corresponded to parcels that synchronized more during the second run and vis versa. Average difference was -0.09 (SD 0.15). In general, the change was relatively small (i.e.<20%) for most regions. Largest changes were seen in lateral OFC and ventral temporal cortex (Fig 5f). These were the same parcels that showed strong tongue movement related synchronizations with mixed, partly opposite patterns between the two runs (Suppl. Fig. S13). Left IEs also showed a marked increase.

Discussion

Here we have presented the results of a novel clustering algorithm that represent brain activity as a series of complex weighted matrices to extract functionally relevant components. The intention for the development of the algorithm was to device a method that could capture, as precisely as possible, the timing and co-ordination of BOLD-signals across different brain regions. Our intention was not specifically to study anticipation and motor movement. We chose to apply the algorithm to motor data since it is known to reliably activate the movement specific regions of the motor cortex (and presumably not much else) (Barch et al. 2013). The motor cortex is one of the most studied regions of the brain and its functions most well understood. Despite this, even the knowledge of its basic organization has recently been updated (Gordon et al. 2023). Clearly, there is still much to be learnt about its organization and functions.
It should be noted that the fMRI data analysed here was not designed to answer questions about the brain's anticipation, timing and anticipatory finetuning of motor actions across runs. Despite this fact, we found brain-wide, highly regular patterns of cross-subject

synchronizations in activation reflecting these aspects. That task activity induces brain-wide time-locked activations in fMRI has been convincingly shown before by averaging unusually high number of runs (100 runs per subject, 3 subjects) to increase the signal to noise ratio (Gonzalez-Castillo et al. 2012). That approach, using a visual stimulation and letter/number discrimination task, revealed task-locked positive and negative BOLD responses depending on brain region. In most instances they lasted beyond the trial time and in some instances where more prominent post-trial. In many ways, our results are an extension and generalization of that seminal work. However, the method is the opposite with the use of a single run (the two runs are analysed separately) in a relatively large cohort (381 subjects). We believe that a key to the results presented here is the use of the empirical mode decomposition (EMD) algorithm (Huang et al. 1998) which extracts the IMFs. We have previously used the EMD for rs-fMRI data (Strindberg et al. 2021). Applying it to task data highlights its noise reducing and feature extracting powers.

Entrainment

The blocked motor task paradigm clearly enforced a stimulus driven rhythm onto the BOLD-signal response of most of the brain. This phenomena is known as entrainment and is well know from EEG and MEG studies (Herbst and Landau 2016). Entrainment plays a role in selective attention and temporal expectation. It is usually seen in the lower frequency bands (0.1-4(7) Hz) and is potentially an effect of utilizing the brains inherent rhythms for the purpose of task execution (Herbst and Landau 2016; Nobre and Van Ede 2018). In our results, entrainment was not only present in the widespread synchronizations timed to the task paradigm but also as a peak in the power spectrums of bots IMFs corresponding to a15s period which was the exact length of a cue + task block (Suppl. Fig S3). A small number of fMRI studies have investigated entrainment in fMRI. These studies have typically found engagement of the basal ganglia and the precentral gyrus including the SMA (Li et al. 2019; Trost et al. 2014). We are not aware of any other study showing brain wide entrainment in fMRI.

CNV and RP like signals

Our results also show what we interpret to be the fMRI equivalents of CNVs and RPs. The CNV-like signals were seen as pre-cue deflections in non-somatomotor regions. They were also present prior to tasks in motor and somatosensory regions not responsible for the action implementation of the up-coming task. Since the task-paradigm timing was fixed, the preceding task has the function as preparatory cue for the subsequent task. This would explain the emergence of CNV-like responses in the absence of an explicit preparatory cue (Brunia, Van Boxtel, and Böcker 2011). When parcels were to be implicated in the up-coming action, RP-like responses were seen instead. The RP-like responses started earlier, had longer durations and higher amplitude than the CNV-like signals. They were part of an overall higher amplitude, slower IMF waveform in anticipation of and response to motor activity. The RPs and CNVs registered in neurophysiological recordings typically start 0.5-2s prior to task. In the IMF3 timeseries from the motor task data used here, these responses started up to 12 s prior to task, i.e. at the start of the preceding block. The averaged nadir was seen right before cue and the same time that the activation from the preceding task peaked. This meant that there was maximal segregation between the parcels responsible for the current and upcoming and

tasks at the cusp of the new cue. Also, since synchronizations lasted approximately three blocks, at any given timepoint there were three active responses that sometimes interacted. Anticipation and entrainment together seemed to play a role to explain the presence of CNV and RP-like signals. CNV and RP-like signal were also seen in the faster frequency range of IMF2. In IMF2, the timing was different in that it lagged the IMF3 response as the nadir (peak of the deflection) were seen during cue. Given the slow response of the hemodynamic response function, the mechanism causing this effect still originated prior to the cue.

Interestingly, for some parcels in the somatosensory cortex we noted a reduction in the amplitudes of the CNVs in the second run prior to non-parcel specific motor tasks. We interpret this as a potential learning effect between the two runs. If this is correct, it would mean that the somatosensory cortex is involved in motor planning and anticipation, a role that has traditionally been assigned to the premotor cortex. The order in which the blocks appeared in the second run shared some of the same structure as the first run in terms of meta-blocks; The order within the meta-blocks were preserved but the meta-blocks were run in the reverse order the second time. It is unlikely that participants had actively memorized the order and were making active guesses. It seems more plausible that the brain subconsciously had registered the paradigm structure which was utilized as a prior probability in the upcoming anticipations. It is also possible that the learning of semi-repeated task paradigm structure was enhanced by the two previous trials of WM and gambling which participants had engaged in right before the two motor tasks (Bader and Wiener 2023). While a subconscious learning effect/fine-tuning between runs might contribute to some of the results, it does not explain the specificity of the RP-like responses. One would expect the RP like synchronizations to be less specific in the beginning of each run due to higher degree of uncertainty as a function of more choice between possible next movements. It should similarly be stronger towards the end of each run when choice between motor movements were less, especially during the second half of each run. Neither was seen. The subjects in this dataset did not choose which movement to do and when. In a strict sense therefor, the RP-like signal should perhaps be classified as an intensified CNV-like response (Armstrong, Sale, and Cunnington 2018). However, if RPs and CNVs are distinct phenomena remains to be clarified. Also, given that subjects where aware that they would perform each motor task twice within a run, one could expect to find a build-up of CNV-like signals prior to each task in regions of somato-motor cortex responsible for tasks not yet performed or only performed once. While small amplitude, CNV-like signals were seen prior to most (but not all) blocks and in most (but not all) movement specific parcel, they remained constant in size and did not reflect mounting expectation as function of increased probability. The exception of gradually increasing CNV-like signals were seen in the first run in the same somatosensory parcels that in the second run had reduced inter-task synchronizations. The origin and meaning of the CNV-like signals are likely multifactorial. Further studies are needed to disentangle their properties.

Timescales of anticipatory signals in M/EEG and fMRI

M/EEG source localization is challenging due to the inverse problem of trying to estimate cortical (and subcortical) sources from mixed signals. This means that the localization of sources comes with a non-trivial amount of uncertainty. fMRI has the advantage of much

better spatial precision and a comparatively stronger signal to noise ratio. Our results indicate that the BOLD signals have similar preparatory responses to expectation as seen in M/EEG. Interestingly, these signs of anticipation are pervasive and engage most of the brain. While we have focused on the group level results, the method itself by way of the synchronizations timeseries, allows us to infer that the anticipator response is present also at the individual level. This is also apparent by simply looking at individual IMF time series. In contrast, in M/EEG, on has to average over 30-40 trials for the slow negative potentials to be apparent (Brunia, Van Boxtel, and Böcker 2011). The timescales are also somewhat different. While the RPs are typically reported to start up to 2s prior to motor action, in IMF3 the averaged deflection began up to 12s, but more commonly 6s, prior to movement while the CNV-like deflections typically start approximately 6s prior to task. However, the synchronization itself in many instances began already during the positive phase. In IMF2, the pattern was more complex. For most parcels the deflection was timed to the cues. However, in some visual parcels, each peak was followed by a larger deflection that plateaued which corresponded to sudden cross-subject desynchronization after which a smaller deflection with nadir during cue is presents itself (Suppl. Fig S13). Given that it is uncontroversial that the BOLD signal is coupled to neuronal activity, the results presented here could be used as an interesting starting point to further clarify the cross-frequency relationships with neurophysiological recordings.

Increased synchronization during fixation

The SMA is implicated in motor planning. Its activity has been shown to be stronger in response to free choice actions rather than cued actions using fMRI (Travers 2020, Zappoli 2018, Haggard 2008). It has therefore been suggested that the SMA is more active when the timing of an event is uncertain. The SMA-parcels were bilaterally strongly correlated in their synchronization pattern and with parcels known, in different contexts, as either the cingulo-opercular (CON) or timing network (TN) (Naghibi et al. 2024; D'Andrea et al. 2023)). Together with a subset of this network (right precentral sulcus, right SMG and left inferior precentral sulcus), the SMA showed a pattern of strongest synchronizations right at the first block and at the end of the fixation periods. It then tapered of gradually between those periods of heightened uncertainty (Fig 5c). In our results, activity seemed to increase not necessarily as a response to uncertainty of timing since the timing of the paradigm was static within runs. Rather it seemed to respond more when the brain was not already pre-occupied with another task but in a waiting state of heightened anticipation. Previous reports using different methodologies have shown that the dACC, anterior insula and anterior operculum are active in sustained task activity and at start stop cues (Dosenbach et al. 2006). Here we did see sustained cross subject synchronization across all tasks for the dACC, pre-SMA, anterior insula. However, patterns of sustained synchronizations were also seen for sections of the thalamus, VAN and most of the visual networks as well. The frontal operculum was notable in that it belonged to the few parcels that consistently did not synchronize (See Parcel 87 and 190 in Appendix B,C). Perhaps surprisingly, we did not find task specific responses of SMA and other premotor regions. Nor did we find that their group level synchronization pattern preceded that of the primary motor cortex. However, it is possible that this is a result of the smearing effect of the group level analysis. With a few exceptions notably in the OFC, there was not any obvious temporal ordering of the synchronization timeseries within IMFs. However, IMF2 synchronizations were lagging slightly in relation to IMF3.

Synchronization timeseries reflected the time intervals within which subjects synchronized. This means that the effect of late and early activations in different individuals was represented together. The overlap of the time courses indicates that variability among subjects exists, which was also seen in the raw data. The phase clustering algorithm is designed to answer question of temporal order and timing and could be applied on the individual level. However, single subject analysis was beyond the scope of the present work.

The SMA responses were the opposite to the desynchronization response during fixation seen in many regions of the visual and dorsal attention networks. When visual cues were present, the visual regions showed sustained oscillatory response time-locked to the paradigm but desynchronized during fixation. During fixation they seemed to lose track of the expected timing of the up-coming cue.
Interestingly, one parcel of the visual cortex showed synchronization during the first run but not the second. Weather this has any significance and would be reproducible remains to be seen. Other parts of the brain did show uniform entrainment throughout the run. These belonged to the VAN, FPN and thalamus. In contrast, parts of the basal ganglia had some movement specific synchronizations (tongue movements) while others showed patters of waxing and waning synchronization with either three or four periods of increased synchronization. Given that the basal ganglia are implicated in motor control, this response likely have meaning, but it necessitates a different study to elucidate what it might be. Unsurprisingly given that the DMN is known to decouple during task performance, large parts (but not all) of the DMN showed limited synchronization across subjects.

Tongue associated synchronizations

We found unexpectedly that the tongue synchronized with the temporal poles, frontal poles, OFC, basal ganglia (ventral and middle caudatus) and vmPFC during tongue movement. These synchronizations were both of integration type (in-phase) and segregation type (anti-phase). We were not successful in finding similar previous accounts in the literature. It does not necessarily imply they do not exist but might be rare. It is also possible that our method, not being sensitive to amplitude per see but to phase, is more sensitive than pervious methods and extracts regularities that might have been missed before. However, IMF amplitudes for most of these responses were quite striking. Therefore, it could be that the use of the EMD which is not the standard for fMRI, is key to this finding. Other explanations are also possible. Given that tongue movement might induce an altered breathing pattern, we considered if breath holding could be a potential cause. However, a study investigating the effect of breath holding on a lexical task (i.e. also involving tongue movements), the OFC seemed to be mostly spared from effects induced form the breath holding itself (Birn et al. 2009). It is unlikely therefor that changed breath should explain our findings. While we have not investigated it, it does remain a possibility that subtle head movements resulting from moving the tongue might be implicated. Based on the literature, we made some brief speculations what the tongue-temporal pole-frontal pole-OFC-vmPFC coupling mean. The temporal poles have been shown to be implicated in a wide range of cognitive functions including autobiographical memory, semantic processing, social cognition and complex visual tasks (Herlin,

Navarro, and Dupont 2021). In the present context, it is possible that the synchronizations with the temporal poles were mediated by an implicit association between tongue movement and spoken language. The actual roles of the OFC and vmPFC are still not completely understood (which is the case for most of the brain). They has been shown to be implicated in reward, non-reward, emotion processing, motivation, pleasant sensations, interoception and more (Barrett 2016; Rolls, Cheng, and Feng 2020; Protopopescu et al. 2005; Stalnaker, Cooch, and Schoenbaum 2015). The OFC also contain a secondary taste cortex (Rolls 2004, 2). It's possible therefor that the activation could be related to taste. As for all sensory modalities, the experience of taste and texture are judged as unpleasant, pleasant or neutral. The tongue associated synchronizations could reflect this categorical valance. To answer the question whether the associations between tongue movements and temporal pole, OFC, frontal poles and vmPFC were merely data specific or indicate a more general relationship, the same analysis must be extended to other datasets.

Conclusion

While we have analysed motor data only, it is plausible that most of the non-task specific activations will be seen in other task paradigms that use visual cues, albeit with some modifications. We hope that our results further highlight the importance of the whole brain, dynamic perspective when trying to understand how the brain works. This means that we should not limit our analysis to networks of peak activity during a limited time window but investigate the context in which they appear and dissolve, i.e. the whole brain during whole runs. Our results strongly support the understanding that no part of the brain is an island and that intermittent decrease in signal is an inherent part of neuronally coupled activity, whether it be internally initiated or entrained in conjunction with the external world, or both (Varela et al. 2001).

Beyond the specific results of the data in this study, we have introduced a novel clustering algorithm for complex weighted networks. We hope to have shown its capacity to extract phase consistent (i.e. homogenous) clusters in time-series data across different thresholds. However, the method is not limited to time series but can be used on any network with complex weights. Adjusting the threshold for the phase consistency will yield larger or smaller number of clusters which represent different components of the data. As such it is a general method that potentially could find usability in other fields. We also used our algorithm to show that, with the IMFs as a basis, the brain's functional structure as measured with the BOLD signal, fulfils the criteria for the important notion of structural balance.

Code availability

All code will be made available at zenodo.org and GitHub.

(Pictures 3-6 in this version are temporary)

References

Armstrong, Samuel, Martin V. Sale, and Ross Cunnington. 2018. 'Neural Oscillations and the Initiation of Voluntary Movement'. *Frontiers in Psychology* 9 (December):2509. https://doi.org/10.3389/fpsyg.2018.02509.

Bader, Farah, and Martin Wiener. 2023. 'Neuroimaging Signatures of Metacognitive Improvement in Sensorimotor Timing'. *The Journal of Neuroscience*, December, JN-RM-1789-22. https://doi.org/10.1523/JNEUROSCI.1789-22.2023.

Barabási, Dániel L., Ginestra Bianconi, Ed Bullmore, Mark Burgess, SueYeon Chung, Tina Eliassi-Rad, Dileep George, et al. 2023. 'Neuroscience Needs Network Science'. *The Journal of Neuroscience* 43 (34): 5989–95. https://doi.org/10.1523/JNEUROSCI.1014-23.2023.

Barch, Deanna M., Gregory C. Burgess, Michael P. Harms, Steven E. Petersen, Bradley L. Schlaggar, Maurizio Corbetta, Matthew F. Glasser, et al. 2013. 'Function in the Human Connectome: Task-fMRI and Individual Differences in Behavior'. *NeuroImage* 80 (October):169–89. https://doi.org/10.1016/j.neuroimage.2013.05.033.

Barrett, Lisa Feldman. 2016. 'The Theory of Constructed Emotion: An Active Inference Account of Interoception and Categorization'. *Social Cognitive and Affective Neuroscience*, October, nsw154. https://doi.org/10.1093/scan/nsw154.

Birn, Rasmus M., Kevin Murphy, Daniel A. Handwerker, and Peter A. Bandettini. 2009. 'fMRI in the Presence of Task-Correlated Breathing Variations'. *NeuroImage* 47 (3): 1092–1104. https://doi.org/10.1016/j.neuroimage.2009.05.030.

Böttcher, Lucas, and Mason A. Porter. 2024. 'Complex Networks with Complex Weights'. *Physical Review E* 109 (2): 024314. https://doi.org/10.1103/PhysRevE.109.024314.

Brunia, Cornelis H. M., Geert J. M. Van Boxtel, and Koen B. E. Böcker. 2011. *Negative Slow Waves as Indices of Anticipation: The Bereitschaftspotential, the Contingent Negative Variation, and the Stimulus-Preceding Negativity*. Oxford University Press. https://doi.org/10.1093/oxfordhb/9780195374148.013.0108.

Bubic. 2010. 'Prediction, Cognition and the Brain'. *Frontiers in Human Neuroscience*. https://doi.org/10.3389/fnhum.2010.00025.

Buzsáki, György, Adrien Peyrache, and John Kubie. 2014. 'Emergence of Cognition from Action'. *Cold Spring Harbor Symposia on Quantitative Biology* 79:41–50. https://doi.org/10.1101/sqb.2014.79.024679.

Cabral, Joana, Diego Vidaurre, Paulo Marques, Ricardo Magalhães, Pedro Silva Moreira, José Miguel Soares, Gustavo Deco, Nuno Sousa, and Morten L. Kringelbach. 2017. 'Cognitive Performance in Healthy Older Adults Relates to Spontaneous Switching between States of Functional Connectivity during Rest'. *Scientific Reports* 7 (1): 5135. https://doi.org/10.1038/s41598-017-05425-7.

Cartwright, Dorwin, and Frank Harary. 1956. 'Structural Balance: A Generalization of Heider's Theory.' *Psychological Review* 63 (5): 277–93. https://doi.org/10.1037/h0046049.

Clark, Andy. 2013. 'Whatever next? Predictive Brains, Situated Agents, and the Future of Cognitive Science'. *Behavioral and Brain Sciences* 36 (3): 181–204. https://doi.org/10.1017/S0140525X12000477.

D'Andrea, Carolina Badke, Timothy O. Laumann, Dillan J. Newbold, Steven M. Nelson, Ashley N. Nielsen, Roselyne Chauvin, Scott Marek, Deanna J. Greene, Nico U.F. Dosenbach, and Evan M. Gordon. 2023. 'Substructure of the Brain's Cingulo-Opercular Network'. Neuroscience. https://doi.org/10.1101/2023.10.10.561772.

Dosenbach, Nico U.F., Kristina M. Visscher, Erica D. Palmer, Francis M. Miezin, Kristin K. Wenger, Hyunseon C. Kang, E. Darcy Burgund, Ansley L. Grimes, Bradley L. Schlaggar, and Steven E. Petersen. 2006. 'A Core System for the Implementation of Task Sets'. *Neuron* 50 (5): 799–812. https://doi.org/10.1016/j.neuron.2006.04.031.

Fransson, Peter, and Marika Strindberg. 2023. 'Brain Network Integration, Segregation and Quasi-periodic Activation and Deactivation during Tasks and Rest'. *NeuroImage* 268 (March):119890. https://doi.org/10.1016/j.neuroimage.2023.119890.

Friston, Karl. 2010. 'The Free-Energy Principle: A Unified Brain Theory?' *Nature Reviews Neuroscience* 11 (2): 127–38. https://doi.org/10.1038/nrn2787.

Glasser, Matthew F., Stamatios N. Sotiropoulos, J. Anthony Wilson, Timothy S. Coalson, Bruce Fischl, Jesper L. Andersson, Junqian Xu, et al. 2013. 'The Minimal Preprocessing Pipelines for the Human Connectome Project'. *NeuroImage* 80 (October):105–24. https://doi.org/10.1016/j.neuroimage.2013.04.127.

Glerean, Enrico, Juha Salmi, Juha M. Lahnakoski, Iiro P. Jääskeläinen, and Mikko Sams. 2012. 'Functional Magnetic Resonance Imaging Phase Synchronization as a Measure of Dynamic Functional Connectivity'. *Brain Connectivity* 2 (2): 91–101. https://doi.org/10.1089/brain.2011.0068.

Gonzalez-Castillo, Javier, Ziad S. Saad, Daniel A. Handwerker, Souheil J. Inati, Noah Brenowitz, and Peter A. Bandettini. 2012. 'Whole-Brain, Time-Locked Activation with Simple Tasks Revealed Using Massive Averaging and Model-Free Analysis'. *Proceedings of the National Academy of Sciences* 109 (14): 5487–92. https://doi.org/10.1073/pnas.1121049109.

Gordon, Evan M., Roselyne J. Chauvin, Andrew N. Van, Aishwarya Rajesh, Ashley Nielsen, Dillan J. Newbold, Charles J. Lynch, et al. 2023. 'A Somato-Cognitive Action Network Alternates with Effector Regions in Motor Cortex'. *Nature* 617 (7960): 351–59. https://doi.org/10.1038/s41586-023-05964-2.

Harary, Frank. 1953. 'On the Notion of Balance of a Signed Graph.' *Michigan Mathematical Journal* 2 (2). https://doi.org/10.1307/mmj/1028989917.

Herbst, Sophie K, and Ayelet N Landau. 2016. 'Rhythms for Cognition: The Case of Temporal Processing'. *Current Opinion in Behavioral Sciences* 8 (April):85–93. https://doi.org/10.1016/j.cobeha.2016.01.014.

Herlin, Bastien, Vincent Navarro, and Sophie Dupont. 2021. 'The Temporal Pole: From Anatomy to Function—A Literature Appraisal'. *Journal of Chemical Neuroanatomy* 113 (April):101925. https://doi.org/10.1016/j.jchemneu.2021.101925.

Honari, Hamed, Ann S. Choe, and Martin A. Lindquist. 2021. 'Evaluating Phase Synchronization Methods in fMRI: A Comparison Study and New Approaches'. *NeuroImage* 228 (March):117704. https://doi.org/10.1016/j.neuroimage.2020.117704.

Huang, Norden E., Zheng Shen, Steven R. Long, Manli C. Wu, Hsing H. Shih, Quanan Zheng, Nai-Chyuan Yen, Chi Chao Tung, and Henry H. Liu. 1998. 'The Empirical

Mode Decomposition and the Hilbert Spectrum for Nonlinear and Non-Stationary Time Series Analysis'. *Proceedings of the Royal Society of London. Series A: Mathematical, Physical and Engineering Sciences* 454 (1971): 903–95. https://doi.org/10.1098/rspa.1998.0193.

Kononowicz, Tadeusz W, and Trevor B Penney. 2016. 'The Contingent Negative Variation (CNV): Timing Isn't Everything'. *Current Opinion in Behavioral Sciences* 8 (April):231–37. https://doi.org/10.1016/j.cobeha.2016.02.022.

Lancaster, Iatsenko, Pidde, Ticcinelli, and Stefanovska. 2018. 'Surrogate Data for Hypothesis Testing in Physical Systems'. *Physics Reports* 2018 (748).

Li, Qiang, Guangyuan Liu, Dongtao Wei, Ying Liu, Guangjie Yuan, and Gaoyuan Wang. 2019. 'Distinct Neuronal Entrainment to Beat and Meter: Revealed by Simultaneous EEG-fMRI'. *NeuroImage* 194 (July):128–35. https://doi.org/10.1016/j.neuroimage.2019.03.039.

Naghibi, Narges, Nadia Jahangiri, Reza Khosrowabadi, Claudia R. Eickhoff, Simon B. Eickhoff, Jennifer T. Coull, and Masoud Tahmasian. 2024. 'Embodying Time in the Brain: A Multi-Dimensional Neuroimaging Meta-Analysis of 95 Duration Processing Studies'. *Neuropsychology Review* 34 (1): 277–98. https://doi.org/10.1007/s11065-023-09588-1.

Niazy, Rami K., Jingyi Xie, Karla Miller, Christian F. Beckmann, and Stephen M. Smith. 2011. 'Spectral Characteristics of Resting State Networks'. In *Progress in Brain Research*, 193:259–76. Elsevier. https://doi.org/10.1016/B978-0-444-53839-0.00017-X.

Nobre, Anna C., and Freek Van Ede. 2018. 'Anticipated Moments: Temporal Structure in Attention'. *Nature Reviews Neuroscience* 19 (1): 34–48. https://doi.org/10.1038/nrn.2017.141.

Ponce-Alvarez, Adrián, Gustavo Deco, Patric Hagmann, Gian Luca Romani, Dante Mantini, and Maurizio Corbetta. 2015. 'Resting-State Temporal Synchronization Networks Emerge from Connectivity Topology and Heterogeneity'. Edited by Claus C. Hilgetag. *PLOS Computational Biology* 11 (2): e1004100. https://doi.org/10.1371/journal.pcbi.1004100.

Protopopescu, Xenia, Hong Pan, Margaret Altemus, Oliver Tuescher, Margaret Polanecsky, Bruce McEwen, David Silbersweig, and Emily Stern. 2005. 'Orbitofrontal Cortex Activity Related to Emotional Processing Changes across the Menstrual Cycle'. *Proceedings of the National Academy of Sciences* 102 (44): 16060–65. https://doi.org/10.1073/pnas.0502818102.

Rolls, Edmund T. 2004. 'The Functions of the Orbitofrontal Cortex'. *Brain and Cognition* 55 (1): 11–29. https://doi.org/10.1016/S0278-2626(03)00277-X.

Rolls, Edmund T, Wei Cheng, and Jianfeng Feng. 2020. 'The Orbitofrontal Cortex: Reward, Emotion and Depression'. *Brain Communications* 2 (2): fcaa196. https://doi.org/10.1093/braincomms/fcaa196.

Schaefer, Alexander, Daniel S. Margulies, Gabriele Lohmann, Krzysztof J. Gorgolewski, Jonathan Smallwood, Stefan J. Kiebel, and Arno Villringer. 2014. 'Dynamic Network Participation of Functional Connectivity Hubs Assessed by Resting-State fMRI'. *Frontiers in Human Neuroscience* 8 (May). https://doi.org/10.3389/fnhum.2014.00195.

Schurger, Aaron, Pengbo 'Ben' Hu, Joanna Pak, and Adina L. Roskies. 2021. 'What Is the Readiness Potential?' *Trends in Cognitive Sciences* 25 (7): 558–70. https://doi.org/10.1016/j.tics.2021.04.001.

Schurger, Aaron, Jacobo D. Sitt, and Stanislas Dehaene. 2012. 'An Accumulator Model for Spontaneous Neural Activity Prior to Self-Initiated Movement'. *Proceedings of the National Academy of Sciences* 109 (42). https://doi.org/10.1073/pnas.1210467109.

Seth, Anil K. 2013. 'Interoceptive Inference, Emotion, and the Embodied Self'. *Trends in Cognitive Sciences* 17 (11): 565–73. https://doi.org/10.1016/j.tics.2013.09.007.

Stalnaker, Thomas A, Nisha K Cooch, and Geoffrey Schoenbaum. 2015. 'What the Orbitofrontal Cortex Does Not Do'. *Nature Neuroscience* 18 (5): 620–27. https://doi.org/10.1038/nn.3982.

Strindberg, Marika, Peter Fransson, Joana Cabral, and Ulrika Ådén. 2021. 'Spatiotemporally Flexible Subnetworks Reveal the Quasi-Cyclic Nature of Integration and Segregation in the Human Brain'. *NeuroImage* 239 (October):118287. https://doi.org/10.1016/j.neuroimage.2021.118287.

Tian, Yu, and Renaud Lambiotte. 2023. 'Structural Balance and Random Walks on Complex Networks with Complex Weights'. arXiv. http://arxiv.org/abs/2307.01813.

Travers, Eoin, Maja Friedemann, and Patrick Haggard. 2021. 'The Readiness Potential Reflects Planning-Based Expectation, Not Uncertainty, in the Timing of Action'. *Cognitive Neuroscience* 12 (1): 14–27. https://doi.org/10.1080/17588928.2020.1824176.

Trost, Wiebke, Sascha Frühholz, Daniele Schön, Carolina Labbé, Swann Pichon, Didier Grandjean, and Patrik Vuilleumier. 2014. 'Getting the Beat: Entrainment of Brain Activity by Musical Rhythm and Pleasantness'. *NeuroImage* 103 (December):55–64. https://doi.org/10.1016/j.neuroimage.2014.09.009.

Varela, Francisco, Jean-Philippe Lachaux, Eugenio Rodriguez, and Jacques Martinerie. 2001. 'The Brainweb: Phase Synchronization and Large-Scale Integration'. *Nature Reviews Neuroscience* 2 (4): 229–39. https://doi.org/10.1038/35067550.

Zaslavsky, Thomas. 1982. 'Signed Graphs'. *Discrete Applied Mathematics* 4 (1): 47–74. https://doi.org/10.1016/0166-218X(82)90033-6.